

# Antiferromagnetic Skyrmion-Based Logic Gates Controlled by Electric Currents and Fields

Xue Liang,<sup>1, 2, †</sup> Jing Xia,<sup>2, †</sup> Xichao Zhang,<sup>2</sup> Motohiko Ezawa,<sup>3</sup> Oleg A. Tretiakov,<sup>4</sup>  
Xiaoxi Liu,<sup>5</sup> Lei Qiu,<sup>1, 2</sup> Guoping Zhao,<sup>1, \*</sup> and Yan Zhou<sup>2, \*</sup>

<sup>1</sup>*College of Physics and Electronic Engineering, Sichuan Normal University, Chengdu  
610068, China*

<sup>2</sup>*School of Science and Engineering, The Chinese University of Hong Kong, Shenzhen,  
Guangdong 518172, China*

<sup>3</sup>*Department of Applied Physics, University of Tokyo, Hongo 7-3-1, Tokyo 113-8656, Japan*

<sup>4</sup>*School of Physics, The University of New South Wales, Sydney 2052, Australia*

<sup>5</sup>*Department of Electrical and Computer Engineering, Shinshu University, Wakasato 4-17-1,  
Nagano 380-8553, Japan*

(Dated: September 24, 2019)

†These authors contributed equally.

Corresponding Authors

\*(G.Z.) E-mail: zhaogp@uestc.edu.cn

\*(Y.Z.) E-mail: zhouyan@cuhk.edu.cn

## ABSTRACT

Antiferromagnets are promising materials for future spintronic applications due to their unique properties including zero stray fields, robustness versus external magnetic fields and ultrafast dynamics, which have attracted extensive interest in recent years. In this work, we first investigate the dynamics of isolated skyrmions in an antiferromagnetic nanotrack with a voltage-gated region. It is found that the skyrmion can be jointly controlled by the driving current and the voltage-controlled magnetic anisotropy gradient. We further propose a new design of logic computing gates based on the manipulation of antiferromagnetic skyrmions, which is numerically realized combining several interactions and phenomena, including the spin Hall effect, voltage-controlled magnetic anisotropy effect, skyrmion-skyrmion interaction, and skyrmion-edge interaction. The proposed logic gates can perform the basic Boolean operations of the logic AND, OR, NOT, NAND and NOR gates. Our results may be useful for designing future in-memory logic computing devices with ultra-low energy consumption and ultra-high storage density.

**KEYWORDS:** *Magnetic skyrmion, antiferromagnet, logic gate, spintronics, micromagnetics*

Antiferromagnetic (AFM) materials are abundant in nature,<sup>1-5</sup> which include certain oxides, sulfides and halogen compounds of elements of the iron group, such as FeO, MnO, Cr<sub>2</sub>O<sub>3</sub>, FeS, and FeF<sub>2</sub>. In an AFM system, there are two interpenetrating sublattices, and the magnetic moments of both sublattices are equal in magnitude and coupled by the inter-sublattice exchange interaction.<sup>6</sup> Below the Néel temperature, adjacent magnetic spins are completely aligned in an anti-parallel configuration, leading to zero net magnetization of the system at the macroscopic scale.

An ideal AFM system is insensitive to external magnetic fields and has no stray field.<sup>4, 5, 7-9</sup> Such a feature may improve the stability and reliability of spintronic devices made of AFM materials, in particular against the detrimental effect of magnetic field perturbations.<sup>4</sup> However, the insensitivity of AFM materials to external magnetic fields also makes them hard to be controlled by magnetic fields, which is a method usually applied to ferromagnetic (FM) systems. Due to the zero net magnetization, it is also difficult to observe the AFM spin textures by some conventional experimental techniques, such as using the magneto-optical Kerr effect (MOKE) microscope.<sup>10</sup>

For these reasons, although AFM materials were discovered early in the 1930s,<sup>1</sup> they are not immediately favored by researchers until the observation or realization of the spin pumping effect,<sup>7, 8</sup> spin Hall effect,<sup>2, 11</sup> spin Seebeck effect,<sup>12, 13</sup> and spin-orbit torques<sup>2, 14, 15</sup> in AFM devices in recent years. Nowadays, it has also been found that in the spin-orbitronics,<sup>7</sup> an emerging direction of spintronics, the magnetic order in AFM materials can be electrically controlled and read-out,<sup>2, 9, 16-18</sup> which provide effective ways to realize AFM spintronic devices.

On the other hand, recent spintronics research has focused on magnetic skyrmions,<sup>19-21</sup> which are topologically nontrivial spin configurations and are promising for building future magnetic storage and computing devices due to their nanoscale size, good stability and ultra-low depinning current density.<sup>21-27</sup> Skyrmions have been experimentally observed in various material systems, including ferromagnets,<sup>20, 26, 28-33</sup> semiconductors,<sup>34</sup> ferrimagnets,<sup>35</sup> multiferroic<sup>36</sup> and ferroelectric materials.<sup>37</sup> Recently, several theoretical studies have predicted that skyrmions can also exist in AFM systems in the form of either skyrmion lattices or isolated skyrmions.<sup>4, 38-46</sup>

The AFM skyrmion can be regarded as a combination of two antiferromagnetically exchange-coupled FM skyrmions, where one sublattice skyrmion has a topological charge of +1 and the other has a topological charge of -1.<sup>38, 39</sup> Compared with FM skyrmions, AFM skyrmions hold three advantages: 1) the vanishing net magnetization and zero stray field could enable AFM skyrmions to robustly resist the magnetic perturbations and hence make them potential components for satellite and aircraft electronics;<sup>5</sup> 2) AFM skyrmions can move along the direction of driving force without showing the skyrmion Hall effect;<sup>38-41, 46</sup> 3) it has been theoretically predicted that AFM skyrmions could move at an ultra-high speed driven by spin currents.<sup>38-40, 46</sup> Therefore, AFM skyrmions could be ideal information carriers for future spintronic devices, such as the racetrack-type memory<sup>47</sup> and logic computing devices.<sup>40, 48-55</sup>

In this work, we propose a new design of Boolean logic computing gates based on AFM skyrmions, in which the presence and absence of AFM skyrmions represent the binary digit “1” and “0”, respectively. The proposed logic gates can realize the basic Boolean logic operations of AND, OR, NOT, NAND and NOR gates by using the spin Hall effect,<sup>8</sup> the spin transfer torque, the voltage-controlled magnetic anisotropy (VCMA) effect,<sup>56, 57</sup> the skyrmion-skyrmion interaction<sup>58</sup> and the skyrmion-edge interaction<sup>25</sup> simultaneously. It should be noted that the NAND gate is a universal gate and any other logic gates can be implemented by a combination of NAND gates in principle.<sup>53</sup> One of the major features of the proposed logic gates is that the AFM skyrmion maintains a stable structure during the motion from the input side to the output side without the mutual conversion between skyrmion and domain wall, which could reduce the driving current density as well as the energy consumption of the device. The reason is that the current density required to drive domain wall into motion is larger than that of skyrmion. In our model, the spin-polarized current and the VCMA gradient are used as driving forces, which control the velocity and trajectory of AFM skyrmions in a joint manner.

*Logic Computing Gates.* Figure 1 schematically illustrates our proposed logic computing gates based on the manipulation of AFM skyrmions, including a cross-shaped AFM nanotrack and three magnetic tunnel junctions (MTJs) as input and output heads. The heavy metal layer beneath the AFM layer is used to generate spin currents by using the spin Hall effect.<sup>59</sup> The insulator and electrode structures placed on the transverse AFM nanotrack

is used to control the perpendicular magnetic anisotropy (PMA) within the transverse branch. As shown in Figure 1b, the wedge-shaped insulator will give rise to a linear change in PMA due to the VCMA effect,<sup>56,57</sup> leading to a PMA gradient. Namely, the PMA depends on the thickness of the insulator spacer once the gate voltage is applied. As reported in Ref. [41], the PMA gradient can drive AFM skyrmion into motion along a nanotrack effectively, similar to the spin-polarized current and temperature gradient.<sup>39,60</sup> It should be noted that the PMA of the transverse nanotrack is not entirely modified by the gate voltage, and only the region indicated by the blue dashed box in Figure 1c is voltage gated. The PMA of the nanotrack edges remains to be unchanged during all operations, which could better confine skyrmions within the nanotrack and prevent the annihilation of skyrmions at edges, especially at the junction of the transverse and longitudinal branches.

*A Single Skyrmion in the Nanotrack.* Before studying the AFM-skyrmion-based logic gates, we first investigate the basic dynamic behavior of a single AFM skyrmion in a straight nanotrack with a voltage-gated region, where the constant voltage is applied to modify the local PMA magnitude. As shown in Figure 2a-c, the black shaded box denotes the voltage-gated region. Here, we consider that the PMA value  $K_v$  in the voltage-gated region is constant but smaller than that outside of the voltage-gated region. As a consequence, the voltage-gated region serves as a potential well. Similar to FM skyrmions,<sup>61</sup> when an AFM skyrmion driven by the spin current, it moves toward the right direction and approaches the left boundary of the voltage-gated region, its velocity will gradually increase. However, if the AFM skyrmion arrives at the right boundary of the voltage-gated region, its velocity will reduce significantly. The possibility of the AFM skyrmion passing through the voltage-gated region mainly depends on the magnitude of the driving current density as well as the anisotropy difference between the voltage-gated and non-voltage-gated regions.

We define  $\Delta K$  as the difference between the PMA constant  $K_v$  in voltage-gated region and  $K_0$  in the rest region, i.e.,  $\Delta K = K_0 - K_v$ . As shown in Figure 2a-b, for a same value of  $\Delta K$ , the driving force provided by a small spin current is insufficient for the AFM skyrmion to overcome the energy barrier at the right boundary of the voltage-gated region, so that the skyrmion is trapped eventually. However, if a large current density is applied, the skyrmion

will pass through the voltage-gated region successfully. Besides, the diameter of the AFM skyrmion will increase in the voltage-gated region due to the smaller value of PMA. Therefore, when  $\Delta K$  is larger than certain threshold, the skyrmion is not stable in the voltage-gated region and could be converted into a domain wall pair (see Figure 2c). It is worth mentioning that the conversion between a skyrmion and a domain wall pair can be used as a procedure for realizing the duplication of skyrmion.<sup>48, 62-65</sup> Note that the illustration of an AFM skyrmion is given in Figure 2d. Figure 2e shows the working window of the current-driven motion of a single AFM skyrmion in the voltage-gated nanotrack. It can be seen that the critical driving current density  $j_c$  required to drive the AFM skyrmion passing through the voltage-gated region is proportional to  $\Delta K$ . However, when  $\Delta K$  is larger than  $0.3 \times 10^5 \text{ J m}^{-3}$  in our model, the skyrmion will be broken when it moves into the voltage-gated region.

*Two Skyrmions in the Nanotrack.* We proceed to consider the case when two AFM skyrmions are moving in the nanotrack. Due to the presence of the skyrmion-skyrmion repulsion,<sup>25, 58</sup> we find that four different motion behaviors of skyrmions could occur. As shown in Figure 3a-c, the initial spacing between the two AFM skyrmions equals 50 nm, and the right skyrmion is 100 nm away from the left boundary of the voltage-gated region. Similar to the case of only one skyrmion in the nanotrack, the AFM skyrmions will be destroyed if the PMA in the voltage-gated region is smaller than a certain threshold. However, when the two AFM skyrmions are stable in the voltage-gated region, they are intended to move away from each other due to the skyrmion-skyrmion repulsion. When the driving current density is small, both two AFM skyrmions cannot pass through the right boundary of the voltage-gated region due to the insufficient driving forces provided by the spin current. When the applied current density is slightly increased but still smaller than the critical current density  $j_c$  (i.e., the critical current density for a single AFM skyrmion to pass through the voltage-gated region), the right skyrmion trapped at the right boundary will be pushed out of the voltage-gated region by the left skyrmion (see Figure 3b). Indeed, the left skyrmion will stay in the voltage-gated region as long as the current density is smaller  $j_c$ . If the current density is larger than  $j_c$ , both two AFM skyrmions can pass through the voltage-gated region (see Figure 3c).

Figure 3d shows the working window of the current-induced motion of two AFM skyrmions in a nanotrack. Compared with the case of a single AFM skyrmion (see Figure 2e), when the driving current density is smaller than  $j_c$ , the original phase is divided into two phases. The phenomenon that only one AFM skyrmion is outputted when two AFM skyrmions are inputted could be applied in the transmission, modification and replacement of data in the skyrmion-based racetrack memory,<sup>66</sup> as well as in the skyrmion-based logic computing gates, which we will discuss below.

In our proposed model of logic computing gates, the spin-polarized current is applied in the longitudinal nanotrack (i.e., along the  $x$  direction), while the transverse branch has the VCMA gradient. Hence, the AFM skyrmions on both nanotracks can be driven into motion, and the junction area of the longitudinal and transverse branches is a voltage-gated region with lower PMA. When the logic operation of AND gate is realized, the driving current density in the longitudinal nanotrack is smaller than the critical current density  $j_c$ . When the driving current density is larger than  $j_c$ , the logic operation of OR gate can be realized. In the following, we will demonstrate and discuss in detail the AFM skyrmion-based logic computing gates.

*Logic AND and OR Gates.* In Figure 1a, c, the MTJ sensors placed at the left and upper terminals of the AFM nanotracks act as two input sources, and the one placed at the right terminal of the longitudinal nanotrack is an output sensor. As shown in Figure 4a-b, assuming that only one AFM skyrmion is initially created in the input A side, it will first move to the junction area driven by the spin current. If the driving current density is smaller than  $j_c$ , the skyrmion will continue to move to the lower terminal of the transverse nanotrack due to the VCMA gradient, and thus no skyrmion can be detected at the output side (see Figure 4a). However, if the driving current density is larger than  $j_c$ , the AFM skyrmion will successfully arrive at the right terminal of the longitudinal nanotrack, as shown in Figure 4b. Thus, the logic operation of AND gate “ $1 \cdot 0 = 0$ ” and the logic operation of OR gate “ $1 + 0 = 1$ ” can be implemented by manipulating the motion of AFM skyrmions in the proposed model. Similarly, if the AFM skyrmion is initially created at the input B side, it will move downward to the lower terminal when  $j < j_c$  or move to the output side for  $j > j_c$ . So, the logic operation

of AND gate “ $0 \cdot 1 = 0$ ” and the logic operation of OR gate “ $0 + 1 = 1$ ” can also be implemented.

When two AFM skyrmions are separately created in the two input terminals A and B, by controlling the driving current density ( $j < j_c$ ) and the VCMA gradient, the AFM skyrmion from the input A side and the AFM skyrmion from the input B side could arrive at the junction area at the same time. Due to the repulsion between two skyrmions, the right one will be squeezed out of the voltage-gated region by the left one. As a result, the right AFM skyrmion can reach the output side driven by the spin current, while the left one will move to the lower terminal. When  $j > j_c$ , the left skyrmion could annihilate at the junction area due to the geometric confinement (i.e., the skyrmion-edge interaction). Therefore, the logic operation of AND gate “ $1 \cdot 1 = 1$ ” and the logic operation of OR gate “ $1 + 1 = 1$ ” can be implemented. As shown in Figure 4 (see Movie 1 and Movie 2), the trajectories of the two AFM skyrmions are indicated by yellow lines. The corresponding truth tables of the logic AND and OR gates are given in Figure 4c-d. It should be noted that if there are no skyrmions at both two input sides, the output of “0” will be obtained.

*Logic NOT Gate.* The AFM skyrmion-based logic NOT gate is realized by using the structure given in Figure 5a, including two MTJs as the input (the left one) and output (the right one) sensors, and two voltage gates to control the local magnetic anisotropy by the VCMA effect. Note that there is always an AFM skyrmion at the output side initially. As shown in Figure 5b-c, when the binary digit “0” is inputted at the left terminal, an AFM skyrmion will always be confined within the output side in the presence of a small driving current, due to the higher PMA of voltage-gated regions. Hence, the logic operation of the NOT gate “ $\bar{0} = 1$ ” is realized. If the binary data “1” is inputted at the left terminal, when the inputted skyrmion moves to the left side of the output side, the skyrmion in the output side will be squeezed out by the skyrmion-skyrmion repulsion. Indeed, the left skyrmion cannot enter the output side due to the energy barrier induced by the gate voltage. Therefore, the logic operation of the NOT gate “ $\bar{1} = 0$ ” is also realized.

Based on the above design concept, the logic operation of NAND and NOR gates can also be implemented combining the AND and OR gates with the NOT gate, respectively, which are demonstrated in Figure S1 and Figure S2 (see also Movie 3 and Movie 4). It is worth



mentioning that, for the read-out of information, one can take advantage of the AFM MTJ sensor at the output side. A large tunneling anisotropic magnetoresistance (TAMR) effect has been found experimentally in AFM tunneling junction,<sup>67</sup> which makes it possible to indirectly detect AFM skyrmions through MTJ. In addition, when each logic operation is completed, a large current pulse can be applied to erase the AFM skyrmions in the nanotrack. Alternatively, we can also add a vertical track crossing at the output region to transfer the output skyrmions to the external area.

The AFM skyrmion-based logic computing gates have been implemented and demonstrated by micromagnetic simulations, we now discuss the advantages of the proposed design. First, the magnetic skyrmion is a topologically protected spin texture, and due to the AFM nature, the AFM skyrmion is not sensitive to external magnetic fields, so that the AFM skyrmion-based logic computing gates have a strong ability to against external magnetic disturbances. Besides, the magnitude of the required driving current density is about  $10^{10}$  A m<sup>-2</sup>, which means that the energy consumption of the proposed logic gates can be very low. Also, there is no required conversion between AFM domain walls and AFM skyrmions during the logic computing operations. The current-driven AFM skyrmion can move along the direction of driving force without showing the skyrmion Hall effect,<sup>38-41, 45, 46</sup> so the undesired annihilation of skyrmions at nanotrack edges can be naturally avoided.

In conclusion, we have investigated the dynamic behaviors of a single AFM skyrmion and two AFM skyrmions on a straight nanotrack with a voltage-gated region. We also proposed a new design of logic computing gates based on the manipulation of AFM skyrmions, which are able to perform the logic operations of five basic logic gates, including AND, OR, NOT, NAND and NOR gates. Our results can provide useful guidelines for the design and development of future AFM skyrmion-based logic computing devices.

## METHODS

**Simulation Details.** Micromagnetic simulations are performed by using the Object-Oriented MicroMagnetic Framework (OOMMF) with extended Dzyaloshinskii-Moriya interaction (DMI)<sup>68, 69</sup> module.<sup>70</sup> The time-dependent magnetization dynamics is governed by the well-known Landau-Lifshitz-Gilbert (LLG) equation with spin-transfer torque (STT):

$$\frac{d\mathbf{m}}{dt} = -|\gamma|\mathbf{m} \times \mathbf{H}_{eff} + \alpha \left( \mathbf{m} \times \frac{d\mathbf{m}}{dt} \right) + \boldsymbol{\tau}_{STT}, \quad (1)$$

where  $\mathbf{m}(\mathbf{r}) = \mathbf{M}(\mathbf{r})/M_s$  is the normalized magnetization,  $\mathbf{H}_{eff} = -\delta\epsilon/(\mu_0\delta\mathbf{m})$  is the effective field associated with various energies, such as the exchange energy, the magnetocrystalline anisotropic energy and the DMI energy,  $\gamma$  and  $\alpha$  are the gyromagnetic ratio and damping coefficient, respectively. Rewriting the STT limited to driving current leads to

$$\boldsymbol{\tau}_{STT} = \gamma H_D \mathbf{m} \times (\mathbf{m} \times \mathbf{m}_p), \quad (2)$$

where  $H_D = \hbar P j / (2\mu_0 e M_s t_z)$  is the effective field induced by the applied driving current,  $P$  and  $\mathbf{m}_p$  are, respectively, the spin polarization rate with default value of 0.4 and the unit electron polarization direction set as  $\mathbf{e}_y$  to drive the AFM skyrmion,  $\hbar$  is the Planck constant,  $\mu_0$  is the permeability of vacuum,  $e$  is the electron charge,  $j$  represents the driving current density and  $t_z$  is the thickness of magnetic film.

We consider a thin film with the easy-axis magnetic anisotropy perpendicular to the  $xy$ -plane and the DMI originating from the broken inversion symmetry at the interface. The interfacial DMI is introduced to stabilize the Néel-type skyrmion.<sup>41</sup> Therefore, the total AFM energy density  $\epsilon$  is a function of  $\mathbf{m}$  specified by<sup>38, 40, 45</sup>

$$\epsilon = A \left[ (\nabla m_x)^2 + (\nabla m_y)^2 + (\nabla m_z)^2 \right] - K m_z^2 + D [m_z (\nabla \cdot \mathbf{m}) - (\mathbf{m} \cdot \nabla) m_z], \quad (3)$$

where  $A$  and  $K$  are the exchange stiffness and the PMA constants, respectively, and the last term denotes the micromagnetic energy density associated with the DMI.

For numerical simulations, the typical magnetic parameters adopted from Ref. [39, 40, 45] are used: saturation magnetization  $M_s = 3.76 \times 10^5 \text{ A m}^{-1}$ , exchange stiffness  $A = -6.59 \text{ pJ m}^{-1}$ , DMI constant was fixed at  $8 \times 10^{-4} \text{ J m}^{-2}$ , PMA constant  $K_0 = 1.16 \times 10^5 \text{ J m}^{-3}$ , and Gilbert damping coefficient  $\alpha = 0.1$ . The default mesh size of  $1.0 \times 1.0 \times 0.4 \text{ nm}^3$  is employed to

discretize the AFM film, which is sufficiently smaller than the exchange length  $l_{ex} = \sqrt{A/K} = 7.5 \text{ nm}$  and the skyrmion size to ensure the numerical accuracy.

In all simulations, the AFM skyrmion is generated initially by applying a 0.02-ns-long spin-polarized current pulse of density  $j_0 = 2.0 \times 10^{15} \text{ A m}^{-2}$  and polarization  $P = 0.4$  along  $-z$ -direction. After the current removed, the stable/metastable AFM skyrmion can be obtained by relaxation. In addition, all the modifications of PMA in our model are achieved by the VCMA effect, which refers to the application of an external electric field to transform the charge accumulation/depletion at the magnet/insulator interface to tune the interfacial PMA.<sup>56, 57</sup>

## **ASSOCIATED CONTENT**

### **Supporting Information**

Demonstration and truth tables for the logic NAND and NOR gates based on AFM skyrmions.  
(PDF)

Movies showing the basic Boolean logic operations of AND, OR, NAND, NOR gates realized by manipulating the skyrmion motion in AFM nanotracks. (ZIP)

## **AUTHOR INFORMATION**

### **Corresponding Authors**

\*(G.Z.) E-mail: zhaogp@uestc.edu.cn

\*(Y.Z.) E-mail: zhouyan@cuhk.edu.cn

### **Author Contributions**

†Xue Liang and Jing Xia contributed equally.

### **Notes**

The authors declare no competing financial interest.

## ACKNOWLEDGEMENTS

X.Z. acknowledges the support by the Presidential Postdoctoral Fellowship of The Chinese University of Hong Kong, Shenzhen (CUHKSZ). M.E. acknowledges the support by the Grants-in-Aid for Scientific Research from JSPS KAKENHI (Grant Nos. JP18H03676, JP17K05490 and JP15H05854) and the support by CREST, JST (Grant Nos. JPMJCR16F1 and JPMJCR1874). O.A.T. acknowledges support by the Cooperative Research Project Program at the Research Institute of Electrical Communication, Tohoku University. X.L. acknowledges the support by the Grants-in-Aid for Scientific Research from JSPS KAKENHI (Grant Nos. 17K19074, 26600041 and 22360122). G.Z. acknowledges the support by the National Natural Science Foundation of China (Grant Nos. 51771127, 51571126 and 51772004) of China, the Scientific Research Fund of Sichuan Provincial Education Department (Grant Nos. 18TD0010 and 16CZ0006). Y.Z. acknowledges the support by the President's Fund of CUHKSZ, Longgang Key Laboratory of Applied Spintronics, National Natural Science Foundation of China (Grant Nos. 11974298 and 61961136006), Shenzhen Fundamental Research Fund (Grant No. JCYJ20170410171958839), and Shenzhen Peacock Group Plan (Grant No. KQTD20180413181702403).

## REFERENCES

- (1) Néel, L. *Science* **1971**, 174, (4013), 985.
- (2) Železný, J.; Wadley, P.; Olejník, K.; Hoffmann, A.; Ohno, H. *Nat. Phys.* **2018**, 14, (3), 220-228.
- (3) Jungwirth, T.; Sinova, J.; Manchon, A.; Marti, X.; Wunderlich, J.; Felser, C. *Nat. Phys.* **2018**, 14, (3), 200-203.
- (4) Baltz, V.; Manchon, A.; Tsoi, M.; Moriyama, T.; Ono, T.; Tserkovnyak, Y. *Rev. Mod. Phys.* **2018**, 90, 015005.
- (5) Jungfleisch, M. B.; Zhang, W.; Hoffmann, A. *Phys. Lett. A* **2018**, 382, (13), 865-871.
- (6) Gomonay, O.; Baltz, V.; Brataas, A.; Tserkovnyak, Y. *Nat. Phys.* **2018**, 14, (3), 213-216.
- (7) Jungwirth, T.; Marti, X.; Wadley, P.; Wunderlich, J. *Nat. Nanotechnol.* **2016**, 11, (3), 231-41.
- (8) Cheng, R.; Xiao, J.; Niu, Q.; Brataas, A. *Phys. Rev. Lett.* **2014**, 113, (5).
- (9) Wadley, P.; Howells, B.; Železný, J.; Andrews, C.; Hills, V.; Campion, R. P.; Novák, V.; Olejník, K.; Maccherozzi, F.; Dhesi, S. S.; Martin, S. Y.; Wagner, T.; Wunderlich, J.; Freimuth, F.; Mokrousov, Y.; Kuneš, J.; Chauhan, J. S.; Grzybowski, M. J.; Rushforth, A. W.; Edmonds, K. W.; Gallagher, B. L.; Jungwirth, T. *Science* **2016**, 351, 587.
- (10) Allwood, D. A.; Xiong, G.; Cooke, M. D.; Cowburn, R. P. *J. Phys. D: Appl. Phys.* **2003**, 36, 2175–2182.
- (11) Zhang, W.; Jungfleisch, M. B.; Jiang, W.; Pearson, J. E.; Hoffmann, A.; Freimuth, F.; Mokrousov, Y. *Phys. Rev. Lett.* **2014**, 113, (19), 196602.
- (12) Uchida, K.-i.; Adachi, H.; Ota, T.; Nakayama, H.; Maekawa, S.; Saitoh, E. *Appl. Phys. Lett.* **2010**, 97, (17), 172505.
- (13) Uchida, K.; Takahashi, S.; Harii, K.; Ieda, J.; Koshibae, W.; Ando, K.; Maekawa, S.; Saitoh, E. *Nature* **2008**, 455, (7214), 778-781.
- (14) Fukami, S.; Zhang, C.; DuttaGupta, S.; Kurenkov, A.; Ohno, H. *Nat. Mater.* **2016**, 15, (5), 535-541.
- (15) Oh, Y.-W.; Chris Baek, S.-h.; Kim, Y. M.; Lee, H. Y.; Lee, K.-D.; Yang, C.-G.; Park, E.-S.; Lee, K.-S.; Kim, K.-W.; Go, G.; Jeong, J.-R.; Min, B.-C.; Lee, H.-W.; Lee, K.-J.; Park, B.-G.

*Nat. Nanotechnol.* **2016**, 11, (10), 878-884.

(16) Bodnar, S. Y.; Smejkal, L.; Turek, I.; Jungwirth, T.; Gomonay, O.; Sinova, J.; Sapozhnik, A. A.; Elmers, H. J.; Klau, M.; Jourdan, M. *Nat. Commun.* **2018**, 9, (1), 348.

(17) Garelo, K.; Avci, C. O.; Miron, I. M.; Baumgartner, M.; Ghosh, A.; Auffret, S.; Boulle, O.; Gaudin, G.; Gambardella, P. *Appl. Phys. Lett.* **2014**, 105, (21), 212402.

(18) Šmejkal, L.; Mokrousov, Y.; Yan, B.; MacDonald, A. H. *Nat. Phys.* **2018**, 14, (3), 242-251.

(19) Rössler, U. K.; Bogdanov, A. N.; Pfeleiderer, C. *Nature* **2006**, 442, (7104), 797-801.

(20) Mühlbauer, S.; Binz, B.; Jonietz, F.; Pfeleiderer, C.; Rosch, A.; Neubauer, A.; Georgii, R.; Böni, P. *Science* **2009**, 323, 915.

(21) Nagaosa, N.; Tokura, Y. *Nat. Nanotechnol.* **2013**, 8, (12), 899-911.

(22) Jonietz, F.; Mühlbauer, S.; Pfeleiderer, C.; Neubauer, A.; Münzer, W.; Bauer, A.; Adams, T.; Georgii, R.; Böni, P.; Duine, R. A.; Everschor, K.; Garst, M.; Rosch, A. *Science* **2010**, 330, 1648.

(23) Sampaio, J.; Cros, V.; Rohart, S.; Thiaville, A.; Fert, A. *Nat. Nanotechnol.* **2013**, 8, (11), 839-44.

(24) Iwasaki, J.; Mochizuki, M.; Nagaosa, N. *Nat. Nanotechnol.* **2013**, 8, (10), 742-7.

(25) Zhang, X.; Zhao, G. P.; Fangohr, H.; Liu, J. P.; Xia, W. X.; Xia, J.; Morvan, F. J. *Sci. Rep.* **2015**, 5, 7643.

(26) Woo, S.; Litzius, K.; Kruger, B.; Im, M. Y.; Caretta, L.; Richter, K.; Mann, M.; Krone, A.; Reeve, R. M.; Weigand, M.; Agrawal, P.; Lemesch, I.; Mawass, M. A.; Fischer, P.; Klau, M.; Beach, G. S. *Nat. Mater.* **2016**, 15, (5), 501-6.

(27) Zhou, Y. *Natl. Sci. Rev.* **2019**, 6, (2), 210-212.

(28) Yu, X. Z.; Onose, Y.; Kanazawa, N.; Park, J. H.; Han, J. H.; Matsui, Y.; Nagaosa, N.; Tokura, Y. *Nature* **2010**, 465, (7300), 901-4.

(29) Yu, X. Z.; Kanazawa, N.; Onose, Y.; Kimoto, K.; Zhang, W. Z.; Ishiwata, S.; Matsui, Y.; Tokura, Y. *Nat. Mater.* **2010**, 10, (2), 106-109.

(30) Heinze, S.; von Bergmann, K.; Menzel, M.; Brede, J.; Kubetzka, A.; Wiesendanger, R.; Bihlmayer, G.; Blügel, S. *Nature Phys.* **2011**, 7, (9), 713-718.

(31) Jiang, W.; Upadhyaya, P.; Zhang, W.; Yu, G.; Jungfleisch, M. B.; Fradin, F. Y.; Pearson, J.



E.; Tserkovnyak, Y.; Wang, K. L.; Heinonen, O.; Velthuis, S. G. E. t.; Hoffmann, A. *Science* **2015**, 349, 283.

(32)Maccariello, D.; Legrand, W.; Reyren, N.; Garcia, K.; Bouzehouane, K.; Collin, S.; Cros, V.; Fert, A. *Nat. Nanotechnol.* **2018**, 13, (3), 233-237.

(33)Zázvorka, J.; Jakobs, F.; Heinze, D.; Keil, N.; Kromin, S.; Jaiswal, S.; Litzius, K.; Jakob, G.; Virnau, P.; Pinna, D.; Everschor-Sitte, K.; Rózsa, L.; Donges, A.; Nowak, U.; Kläui, M. *Nat. Nanotechnol.* **2019**, 14, (7), 658-661.

(34)Münzer, W.; Neubauer, A.; Adams, T.; Mühlbauer, S.; Franz, C.; Jonietz, F.; Georgii, R.; Böni, P.; Pedersen, B.; Schmidt, M.; Rosch, A.; Pfleiderer, C. *Phys. Rev. B* **2010**, 81, (4).

(35)Woo, S.; Song, K. M.; Zhang, X.; Zhou, Y.; Ezawa, M.; Liu, X.; Finizio, S.; Raabe, J.; Lee, N. J.; Kim, S.-I.; Park, S.-Y.; Kim, Y.; Kim, J.-Y.; Lee, D.; Lee, O.; Choi, J. W.; Min, B.-C.; Koo, H. C.; Chang, J. *Nat. Commun.* **2018**, 9, (1).

(36)Seki, S.; Yu, X. Z.; Ishiwata, S.; Tokura, Y. *Science* **2012**, 336, 198.

(37)Das, S.; Tang, Y. L.; Hong, Z.; Goncalves, M. A. P.; McCarter, M. R.; Klewe, C.; Nguyen, K. X.; Gomez-Ortiz, F.; Shafer, P.; Arenholz, E.; Stoica, V. A.; Hsu, S. L.; Wang, B.; Ophus, C.; Liu, J. F.; Nelson, C. T.; Saremi, S.; Prasad, B.; Mei, A. B.; Schlom, D. G.; Iniguez, J.; Garcia-Fernandez, P.; Muller, D. A.; Chen, L. Q.; Junquera, J.; Martin, L. W.; Ramesh, R. *Nature* **2019**, 568, (7752), 368-372.

(38)Zhang, X.; Zhou, Y.; Ezawa, M. *Sci. Rep.* **2016**, 6, 24795.

(39)Barker, J.; Tretiakov, O. A. *Phys. Rev. Lett.* **2016**, 116, (14), 147203.

(40)Xia, H.; Jin, C.; Song, C.; Wang, J.; Wang, J.; Liu, Q. *J. Phys. D* **2017**, 50, (50), 505005.

(41)Shen, L.; Xia, J.; Zhao, G.; Zhang, X.; Ezawa, M.; Tretiakov, O. A.; Liu, X.; Zhou, Y. *Phys. Rev. B* **2018**, 98, (13).

(42)Shen, L.; Xia, J.; Zhao, G.; Zhang, X.; Ezawa, M.; Tretiakov, O. A.; Liu, X.; Zhou, Y. *Appl. Phys. Lett.* **2019**, 114, (4), 042402.

(43)Diaz, S. A.; Klinovaja, J.; Loss, D. *Phys. Rev. Lett.* **2019**, 122, (18), 187203.

(44)Khoshlahni, R.; Qaiumzadeh, A.; Bergman, A.; Brataas, A. *Phys. Rev. B* **2019**, 99, (5).

(45)Zhao, X.; Ren, R.; Xie, G.; Liu, Y. *Appl. Phys. Lett.* **2018**, 112, (25), 252402.

(46)Velkov, H.; Gomonay, O.; Beens, M.; Schwiete, G.; Brataas, A.; Sinova, J.; Duine, R. A. *New J. Phys.* **2016**, 18, (7), 075016.

- (47) Parkin, S. S.; Hayashi, M.; Thomas, L. *Science* **2008**, 320, 190.
- (48) Zhang, X.; Ezawa, M.; Zhou, Y. *Sci. Rep.* **2015**, 5, 9400.
- (49) Luo, S.; Song, M.; Li, X.; Zhang, Y.; Hong, J.; Yang, X.; Zou, X.; Xu, N.; You, a. L. *Nano. Lett.* **2018**, 18, 1180.
- (50) Yu, W.; Lan, J.; Xiao, J. *arXiv:1906.08702v1* **2019**.
- (51) Omari, K. A.; Broomhall, T. J.; Dawidek, R. W. S.; Allwood, D. A.; Bradley, R. C.; Wood, J. M.; Fry, P. W.; Rosamond, M. C.; Linfield, E. H.; Im, M.-Y.; Fischer, P. J.; Hayward, T. J. *Advanced Functional Materials* **2019**, 29, (10), 1807282.
- (52) Rana, B.; Otani, Y. *Phys. Rev. Applied* **2018**, 9, (1).
- (53) Schneider, T.; Serga, A. A.; Leven, B.; Hillebrands, B.; Stamps, R. L.; Kostylev, M. P. *Appl. Phys. Lett.* **2008**, 92, (2), 022505.
- (54) Mankalale, M. G.; Zhao, Z.; Wang, J.-P.; Sapatnekar, S. S. *IEEE Trans. Electron Devices* **2019**, 66, (4), 1990-1996.
- (55) Maverick, C.; Xuan, H.; Felipe, G.-S.; Neilesh, B.; Christoforos, M.; Joseph, S. F. *arXiv:1806.10337v1* **2018**.
- (56) M. Weisheit; Fähler, S.; Marty, A.; Souche, Y.; Poinssignon, C.; Givord, D. *Science* **2007**, 315, 349.
- (57) Maruyama, T.; Shiota, Y.; Nozaki, T.; Ohta, K.; Toda, N.; Mizuguchi, M.; Tulapurkar, A. A.; Shinjo, T.; Shiraishi, M.; Mizukami, S.; Ando, Y.; Suzuki, Y. *Nat. Nanotechnol.* **2009**, 4, (3), 158-61.
- (58) Lin, S.-Z.; Reichhardt, C.; Batista, C. D.; Saxena, A. *Phys. Rev. B* **2013**, 87, (21).
- (59) Sinova, J.; Valenzuela, S. O.; Wunderlich, J.; Back, C. H.; Jungwirth, T. *Rev. Mod. Phys.* **2015**, 87, (4), 1213-1260.
- (60) Chen, Z. Y.; Yan, Z. R.; Qin, M. H.; Liu, J. M. *Phys. Rev. B* **2019**, 99, (21).
- (61) Zhang, X.; Zhou, Y.; Ezawa, M.; Zhao, G. P.; Zhao, W. *Sci. Rep.* **2015**, 5, 11369.
- (62) Zhou, Y.; Ezawa, M. *Nat. Commun.* **2014**, 5, 4652.
- (63) Garg, C.; Pushp, A.; Yang, S. H.; Phung, T.; Hughes, B. P.; Rettner, C.; Parkin, S. S. P. *Nano Lett.* **2018**, 18, (3), 1826-1830.
- (64) Awano, H. *J. Magn. Magn. Mater.* **2015**, 383, 50-55.
- (65) Omari, K. A.; Hayward, T. J. *Phys. Rev. Appl.* **2014**, 2, (4).

- (66)Zhu, D.; Kang, W.; Li, S.; Huang, Y.; Zhang, X.; Zhou, Y.; Zhao, W. *IEEE Trans. Electron Devices* **2018**, 65, (1), 87-95.
- (67)Park, B. G.; Wunderlich, J.; Marti, X.; Holy, V.; Kurosaki, Y.; Yamada, M.; Yamamoto, H.; Nishide, A.; Hayakawa, J.; Takahashi, H.; Shick, A. B.; Jungwirth, T. *Nat. Mater.* **2011**, 10, (5), 347-51.
- (68)Dzyaloshinsky, I. *J. Phys. Chem. Solids* **1958**, 4, 241.
- (69)Moriya, T. *Phys. Rev.* **1960**, 120, (1), 91-98.
- (70)Donahue, M.; Porter, D. G. **1999**, OOMMF User's guide, Version 1.0, Interagency Report No.NISTIR 6376, NIST, Gaithersburg, MD.

## FIGURES

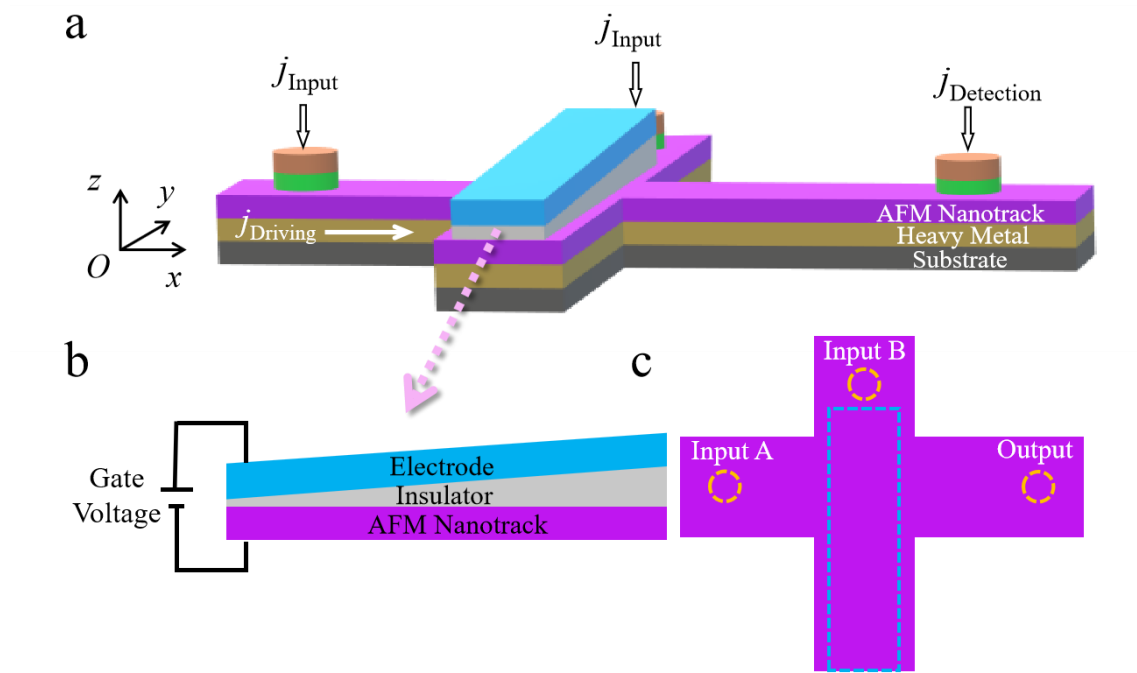


Figure 1. Schematic of the proposed device structure. (a) The 3D illustration of the AFM skyrmion logic AND/OR gates, which has a cross-shaped AFM nanotrack and three MTJs as input and output sensors. (b) Schematic view ( $yz$ -plane) of the transverse nanotrack design. (c) Schematic view ( $xy$ -plane) of the logic gates, where the yellow dashed circles represent the input and output sensors, and the region indicated by the blue dashed box has a PMA gradient along  $-y$ -direction induced by the VCMA effect.

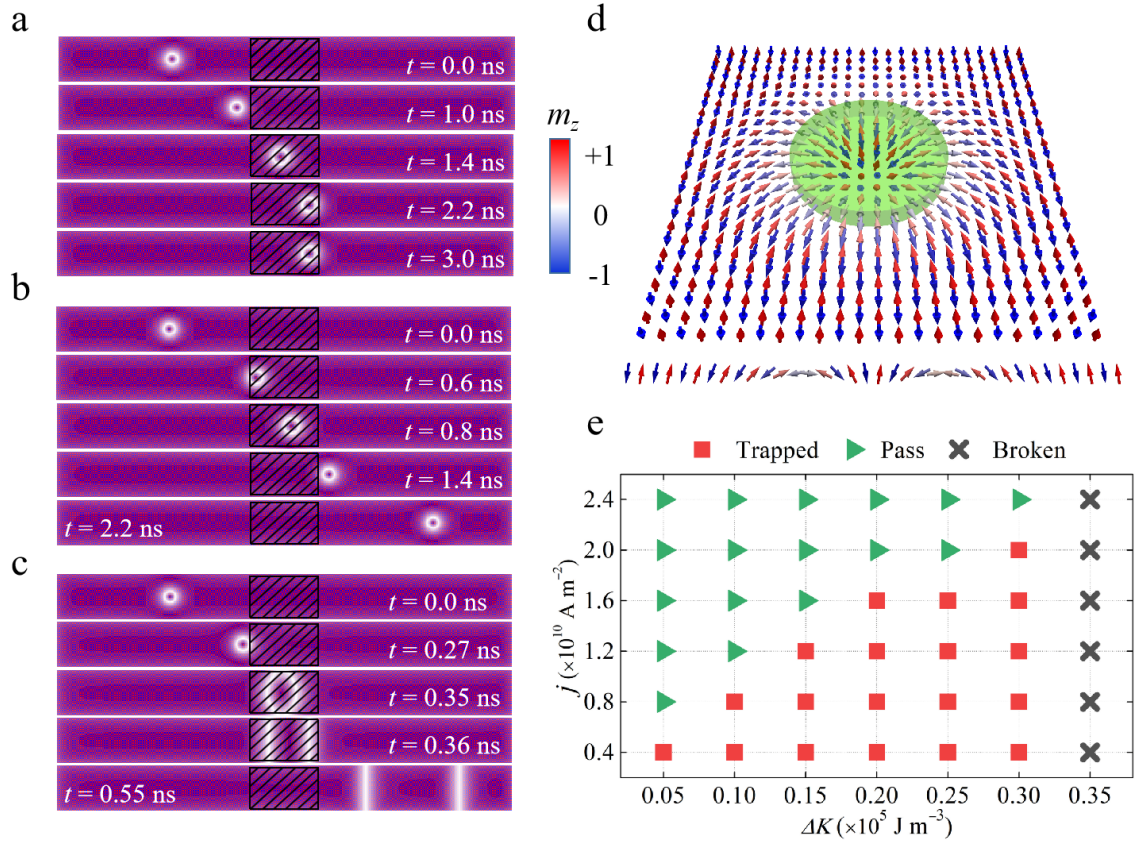


Figure 2. Current-induced motion of a single skyrmion in an AFM nanotrack with a 60-nm-long voltage-gated region. (a)  $j = 1.0 \times 10^{10} \text{ A m}^{-2}$ ,  $\Delta K = 0.2 \times 10^5 \text{ J m}^{-3}$ . (b)  $j = 2.0 \times 10^{10} \text{ A m}^{-2}$ ,  $\Delta K = 0.2 \times 10^5 \text{ J m}^{-3}$ . (c)  $j = 4.0 \times 10^{10} \text{ A m}^{-2}$ ,  $\Delta K = 0.35 \times 10^5 \text{ J m}^{-3}$ . (d) Illustration of an AFM skyrmion spin texture with the two antiparallel magnetic sublattices. The green cylinder denotes the core area of skyrmion. (e) The working window of the current-induced motion of a single AFM skyrmion. The red squares denote the case where skyrmion will be trapped in the voltage-gated region. The green triangles represent the situation where skyrmion can pass smoothly. The black cross indicates that the skyrmion is not stable in the voltage-gated region and could be converted into a domain wall pair. In the simulation, the AFM racetrack with size of  $400 \times 40 \times 0.4 \text{ nm}^3$  is adopted.

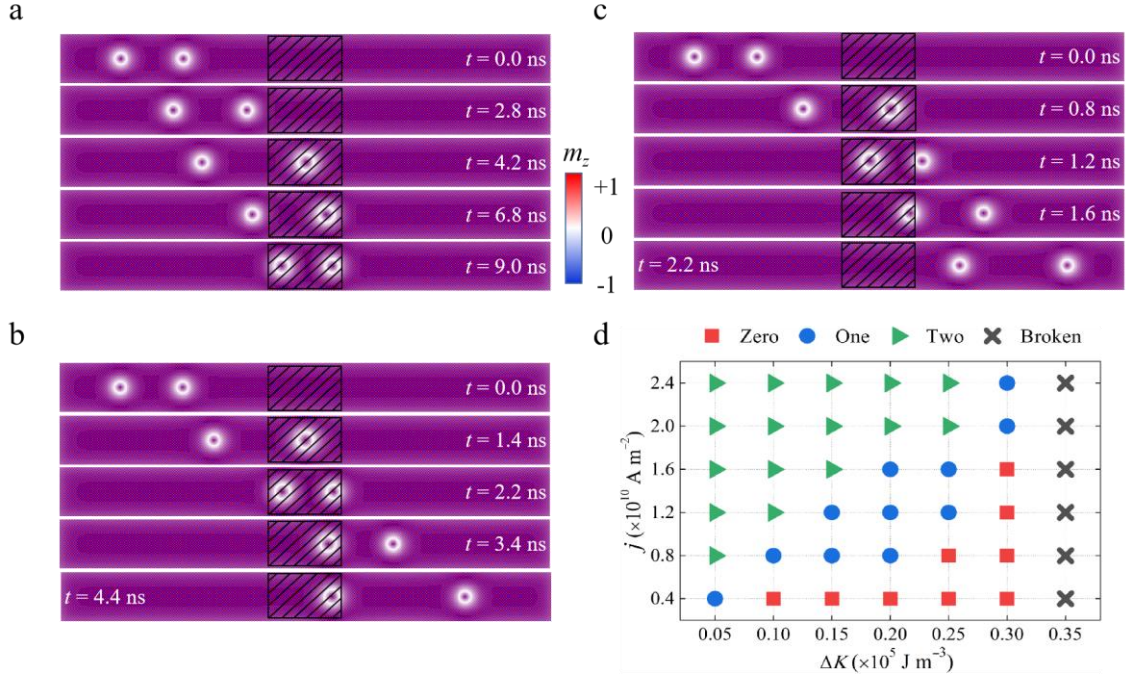


Figure 3. Current-induced motion of two skyrmions in an AFM nanotrack with a 60-nm-long voltage-gated region. (a)  $j = 0.3 \times 10^{10} \text{ A m}^{-2}$ . (b)  $j = 1.0 \times 10^{10} \text{ A m}^{-2}$ . (c)  $j = 2.0 \times 10^{10} \text{ A m}^{-2}$ . (d) The working window of the current-induced motion of two AFM skyrmions. The red squares represent the phase in which no skyrmion can pass the voltage-gated region. The blue circles indicate that the former skyrmion will be pushed out of the gated region, but the latter still be trapped. The green triangles denote that both skyrmions can pass through the voltage-gated region successfully. The black cross indicates that the skyrmion is not stable and could be converted into a domain wall pair. In (a–c), the difference between  $K_v$  and  $K_0$  is fixed at  $0.2 \times 10^5 \text{ J m}^{-3}$ .

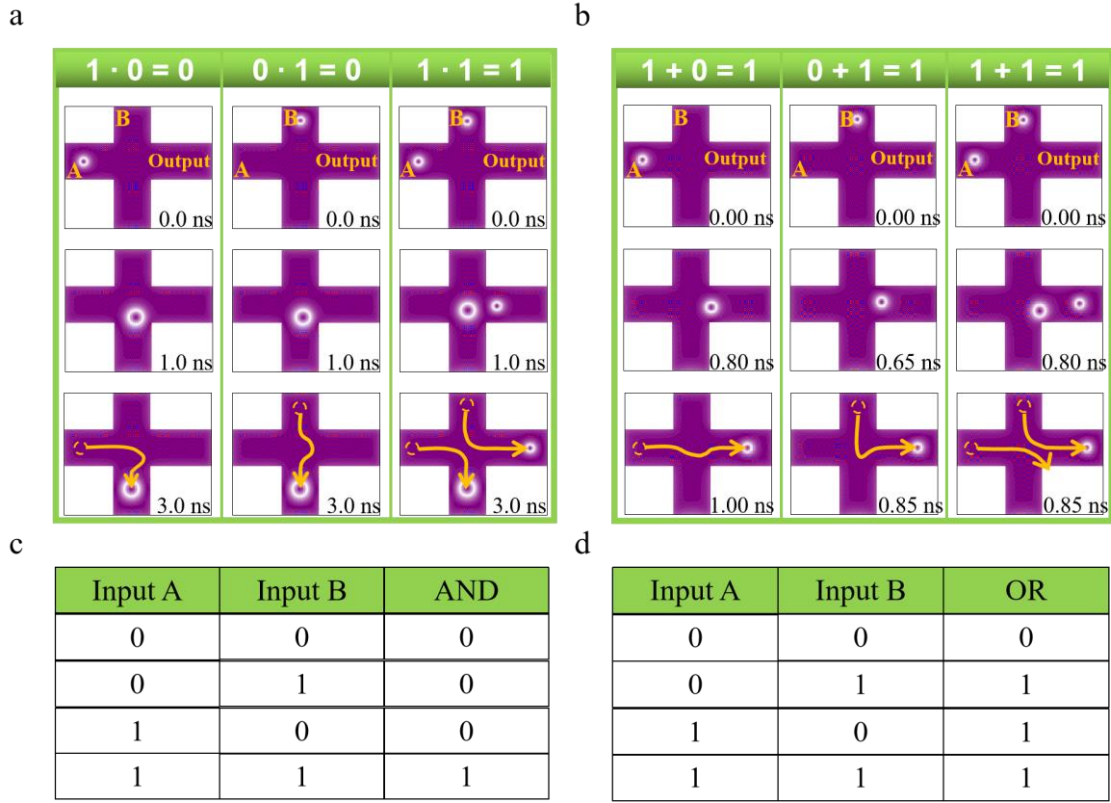


Figure 4. Demonstration of the logic AND and OR gates based on AFM skyrmions. (a–b) The micromagnetic simulations of the three basic logical operations, where the trajectories of skyrmions in AFM nanotrack are identified by yellow lines and the dashed circles represent the initial positions of AFM skyrmions. (c–d) The truth tables of the logic AND and OR gates. In the simulation,  $j = 1.5 \times 10^{10} \text{ A m}^{-2}$ ,  $dK/dy = 400 \text{ GJ m}^{-4}$  and the delay in applying the current is  $\Delta t = 0.4 \text{ ns}$  for AND gate.  $j = 4.0 \times 10^{10} \text{ A m}^{-2}$ ,  $dK/dy = 400 \text{ GJ m}^{-4}$  and  $\Delta t = 0.48 \text{ ns}$  for OR gate.



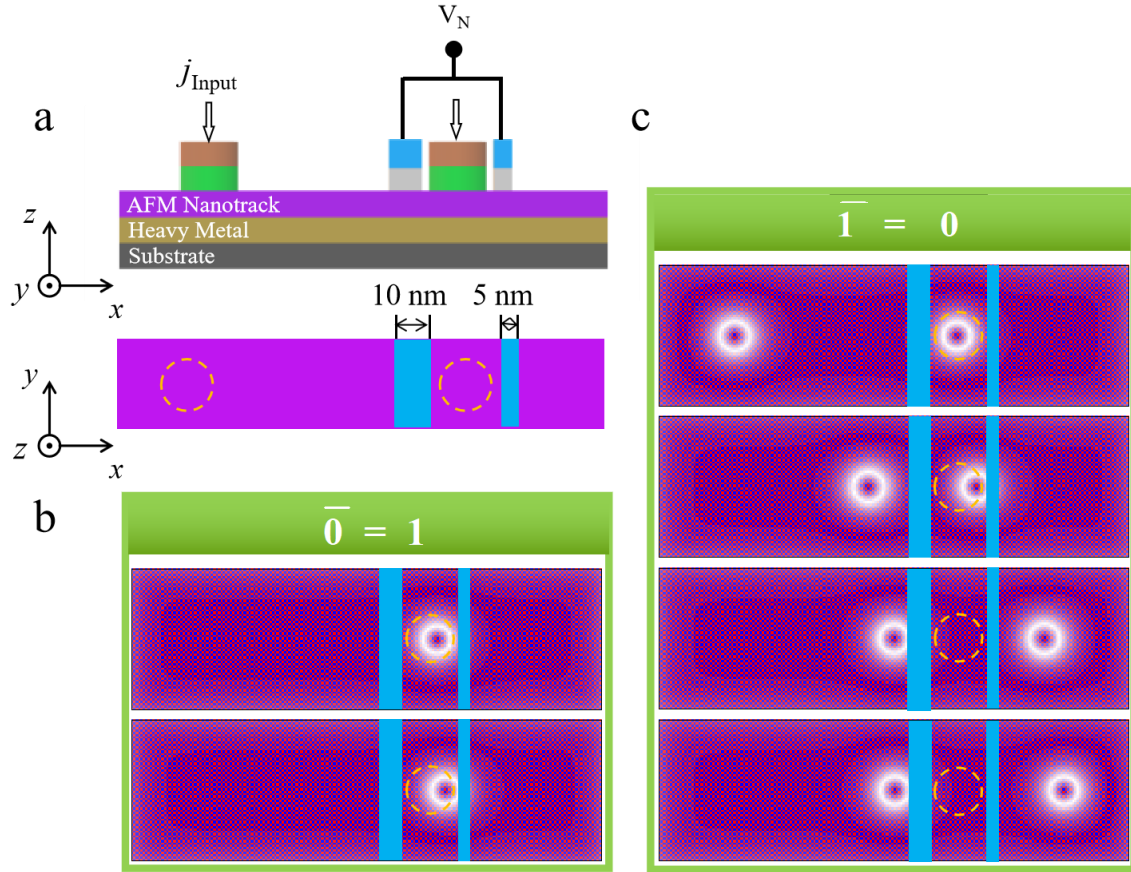


Figure 5. Logic NOT gate based on AFM skyrmions. (a) Illustration of the logic NOT gate, which has a single branch AFM nanotrack, two MTJs as input and output sensors, and two voltage gates on the either side of the output. (b), (c) Demonstration of the logic NOT gate based on AFM skyrmion, where  $j = 1.5 \times 10^{10} \text{ A m}^{-2}$ , and the anisotropy constant  $K_V = 1.5 \times 10^5 \text{ J m}^{-3}$  in the voltage-controlled region.



**FOR TABLE OF CONTENTS ONLY**

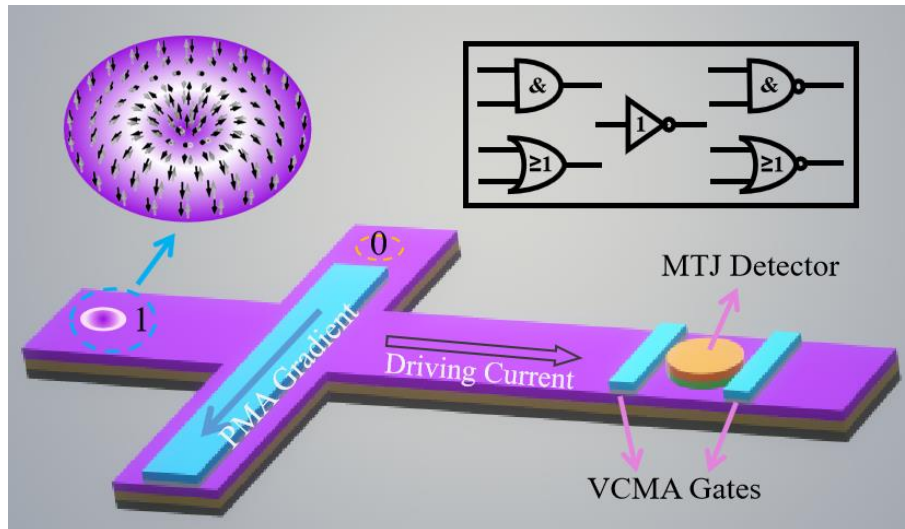


Table of Contents Graphics (6 cm × 3.5 cm)